Influence of Cracks in the Microporous Layer on the Water Distribution in a PEM Fuel Cell Investigated by Synchrotron Radiography

H. Markötter[1)], J. Haußmann[2)], R. Alink[3)], C. Tötzke[1)], T. Arlt[1)], M. Klages[2)], H. Riesemeier[4)], J. Scholta[2)], D. Gerteisen[3)], J. Banhart[1)], I. Manke[1)]

[1)] Helmholtz-Zentrum Berlin (HZB), Hahn-Meitner-Platz 1, 14109 Berlin, Germany
[2)] Zentrum für Sonnenenergie und Wasserstoff-Forschung Baden-Württemberg (ZSW), Helmholtzstraße 8, 89081 Ulm, Germany
[3)] Fraunhofer-Institut für Solare Energiesysteme (ISE), Heidenhofstr. 2, 79110 Freiburg, Germany
[4)] BAM, Bundesanstalt für Materialforschung und -prüfung, Unter den Eichen 87, 12205 Berlin

Water evolution in the gas diffusion layer of a polymer electrolyte membrane fuel cell was visualized *in situ* by means of synchrotron X-ray radiography. Cracks in the microporous layer were identified as start points of efficient liquid water transfer paths through the gas diffusion layer. Quantitative analysis of the water flow rate through those arbitrarily distributed cracks into the gas channel revealed that they have a strong influence on the overall liquid water transport. This could find entry into future material design and simulation.

1. Introduction

Fuel cells are expected to play a major role in a future energy supply chain. With regard to the automotive sector the polymer electrolyte membrane fuel cell (PEMFC) is considered the most promising fuel cell type. Besides cost reduction, water management is a major challenge in the development of PEMFCs [1-4]. A well balanced cell water management must prevent two unfavorable extremes: Membrane drying out and flooding of the diffusion media. In the first case, the membrane shrinks and loses its proton conductivity, which leads to performance loss and membrane degradation. In the second case, liquid water in the cell blocks the gas diffusion layer (GDL). As a consequence, the catalyst layer is undersupplied with gas and the cell performance drops. Hence, a well balanced water management is prerequisite for optimum power output and long term stability. The microstructure of the GDL and the adjacent MPL crucially influence the adjustment of water flow conditions, as smallest details such as cracks in the MPL can significantly affect liquid water transport through the GDL [5]. The size and distribution was detailed studied by Hizir et al. in [6], who found that cracks in the MPL can be accounted for degradation effects, arising due to freeze/thaw cycles. This is attended by delamination of the catalyst layer from the membrane [7].

Neutron radiography has been applied to study the water distribution in PEMFCs *in situ* [8-15]. However, typical spatial resolutions of about 100 µm are too low to resolve the detailed water distribution inside the GDL and MPL. In contrast, synchrotron X-ray radiography is much better suited for the investigation of smaller regions of interest, e.g. water inside GDL pore structure. Typical spatial resolutions are around 1 µm with time resolutions of about 1 s [16-19]. Here we present a quantitative study of the effects of cracks present in the MPL of a PEMFC on water distribution and transport in the cell.

2. Fuel cell

The PEM fuel cell investigated was designed to meet the requirements of synchrotron radiography. In order to achieve sufficient beam transmission and suitable sensitivity to water, holes of 10 mm diameter - corresponding to the field of view - were drilled into the end plates. This implies that only a small part of 0.5 cm² of the active area (44 cm²) is visualized. The vertically aligned channel shown in Fig. 1 has a width of 1 mm. In this part of the channel the gas flow is directed downwards. The cell is equipped with GDLs of type SGL 25BC on both sides, which are 235 µm thick including an MPL. The material contains 5 wt.-% PTFE in the fiber substrate and 23 wt.-% PTFE in the MPL. A Gore Primea 5761 catalyst coated membrane (ccm) with an 18 µm thick membrane was assembled. The anode was loaded with 0.45 mg/cm² Pt/Ru. The cathode with 0.4 mg/cm² Pt. The cell is operated at 50 °C and a current density of 1 A/cm² while being supplied with 0.5 slpm H_2 and 2 slpm air, corresponding to stoichiometric ratios of 1.63 at anode and 2.74 at cathode, respectively. The gases have a dew point of 50 °C and enter the cell at a relative humidity of 100%.

3. Synchrotron radiography setup

The work presented was performed at the BAMline (Bessy II electron storage ring, Helmholtz-Zentrum Berlin, Germany) [20]. A $CdWO_4$ (cadmium tungstenate) scintillator screen was used to convert X-rays into visible light, which is projected onto a 4008×2672 pixel CCD detector (model PCO4000). The field of view is about 8.8×5.9 mm² with a pixel size of 2.2 µm. The exposure time was 5 s. To achieve optimal image contrast the X-ray energy was set to 15 keV using a double multilayer monochromator.

4. Water quantification by means of radiography

During passage through the cell through the plane, the synchrotron beam penetrates a distribution of water, the total amount of which can be expressed by an equivalent effective thickness. To obtain this, all the images were first normalized with respect to an image of the dry cell to extract the attenuation by water from the projection images. The water thickness is then determined by applying Lambert-Beer's attenuation law [21]. As the attenuation coefficient μ for water at the specific beam energy of 15 keV is known (0.15 mm^{-1} [22]), the transmitted water thickness d is calculated as follows:

$$d = -\frac{\ln(I / I_0)}{\mu} .$$
(1)

In equation (1), I denotes the intensity at a certain pixel of the cell in operation, I_0 that of the dry cell. Due to the imaging geometry chosen, the figure d obtained represents all the water in the membrane, the GDLs and the flow field channels of both the anode and cathode side. To quantify the water amount of single droplets the background caused by the water agglomerations in the GDL/channel was subtracted. The background was calculated by analyzing the water amount around the droplets area.

5. Results

The time after the current step from 0 to 1 A/cm² is shown in the image series shown in Fig. 1a-d. Due to the operation of the cell water is formed. It occurs in small amounts in pores all over the GDL, at the channel walls in form of bigger agglomerations, in cracks

of the MPL and in the channel situated at the surface of the GDL (Fig. 1d arrows, see also Fig. 2).

After start of the cell current liquid water is formed within the first few minutes. Cracks in the MPL become visible as they fill up with liquid water. After about 55 s this is the case for two cracks in Fig. 1b (red and green arrow) and after 1 min and 25 s also for a third crack in the center of the image marked with a black arrow. These three cracks are typically 10-20 µm wide and are filled with water over a length ranging from 300 µm to 500 µm.

Due to exposure times of 5 s quickly moving water, e. g. in the channel is motion blurred and gives rise to bright diffuse areas (Fig. 1d, right channel side). As shown in previous investigations [5,23] these cracks are situated in the MPL and might influence transport of liquid water. After filling the cracks in the MPL, droplets arise (Fig. 1c and d, arrows), which are situated on the surface of the GDL above the cracks, as sketched in Fig. 2. It can be assumed that the cracks in the MPL and the droplets in the channel are the start and end points of liquid water transport paths through the GDL.

Water flow rate into one of the droplets (marked with a red arrow in Fig. 1b-d) was calculated. The volume of the droplet is displayed as a function of time in Fig. 3b, which shows that the continuous flow of liquid water into the cracks generates an approximately cyclic process of droplet formation at and detachment of the GDL surface. The droplets grows to a critical size of about 5 nl [nl = $(100 \, \mu m)^3$] before it detaches and is carried away either by the stream of gas or by other droplets that move quickly through the channel. The process is near-periodic with period of 80 s to 120 s. The average droplet growth rate that represents liquid water flow into the droplet is 0.057±0.006 nl/s.

Under the hypothesis that water produced at the cathode is transported through the GDL solely in the liquid state, the electrochemically active area necessary to produce the observed amount of water can be calculated: A circular area with a diameter of 280±15 µm would produce the amount of water that is fed to the observed droplet. However, this assumption is not realistic. The temperature at the cathode catalyst is higher than in other parts of the cell, i.e. the air saturation at the catalyst is below 100 % and a certain amount of water is transported in gaseous form through the GDL subsequently condensing at the channel walls. From the growth rate of the three observed droplets it can be concluded that 6 % of the total water produced in the visualized area is transported in the liquid state through the aforementioned cracks in the MPL. Therefore we can conclude that transport paths starting at MPL cracks strongly affect the overall liquid water transport through the GDL.

6. Summary and Outlook

We presented a study on a PEM fuel cell focusing on the transport of liquid water through the GDL. We found that liquid water is preferably transported along paths starting at arbitrarily distributed MPL cracks. It was shown, that such paths make an important contribution to the overall liquid water transfer through the GDL.

These findings open a new perspective for materials design and optimization since, for example, size, density and structure of MPL cracks could be tailored during production in analogy to other approaches to GDL design, e.g. by perforating GDLs [24,25].

Acknowledgements

References

[1]   W. Vielstich, A. Lamm, H.A. Gasteiger, Handbook of Fuel Cells – Fundamentals, Technology and Applications, Vol. 3, John Wiley & Sons, Chichester, 2003.

[2]   J. Garche, C.K. Dyer, P.T. Moseley, Z. Ogumi, D.A.J. Rand, B. Scrosati, Encyclopedia of Electrochemical Power Sources, Vol. 3, Elsevier, Amsterdam, 2009, pp. 4538.

[3]   L. Carrette, K.A. Friedrich, U. Stimming, Fuel Cells 1 (2001) 5-39.

[4]   C.-Y. Wang, Chem Rev 104 (2004) 4727-4766.

[5]   T. Sasabe, P. Deevanhxay, S. Tsushima, S. Hirai, Electrochem Commun 13 (2011) 638-641.

[6]   F.E. Hizir, S.O. Ural, E.C. Kumbur, M.M. Mench, J Power Sources 195 (2010) 3463-3471.

[7]   S. Kim, B.K. Ahn, M.M. Mench, J Power Sources 179 (2008) 140-146.

[8]   R.J. Bellows, M.Y. Lin, M. Arif, A.K. Thompson, D. Jacobson, J Electrochem Soc 146 (1999) 1099-1103.

[9]   R. Satija, D.L. Jacobson, M. Arif, S.A. Werner, J Power Sources 129 (2004) 238-245.

[10] M.A. Hickner, N.P. Siegel, K.S. Chen, D.S. Hussey, D.L. Jacobson, M. Arif, J Electrochem Soc 155 (2008) 427-434.

[11] D. Kramer, J. Zhang, R. Shimoi, E. Lehmann, A. Wokaun, K. Shinohara, G.G. Scherer, Electrochim Acta 50 (2005) 2603-2614.

[12] P. Boillat, D. Kramer, B.C. Seyfang, G. Frei, E. Lehmann, G.G. Scherer, A. Wokaun, Y. Ichikawa, Y. Tasaki, K. Shinohara, Electrochem Commun 10 (2008) 546-550.

[13] C. Hartnig, I. Manke, N. Kardjilov, A. Hilger, M. Grünerbel, J. Kaczerowski, J. Banhart, W. Lehnert, J Power Sources 176 (2008) 452-459.

[14] A. Schröder, K. Wippermann, J. Mergel, W. Lehnert, D. Stolten, T. Sanders, T. Baumhöfer, D.U. Sauer, I. Manke, N. Kardjilov, A. Hilger, J. Schloesser, J. Banhart, C. Hartnig, Electrochem Commun 11 (2009) 1606-1609.

[15] A. Schröder, K. Wippermann, W. Lehnert, D. Stolten, T. Sanders, T. Baumhöfer, N. Kardjilov, A. Hilger, J. Banhart, I. Manke, J Power Sources 195 (2010) 4765-4771.

[16] I. Manke, C. Hartnig, M. Grunerbel, W. Lehnert, N. Kardjilov, A. Haibel, A. Hilger, J. Banhart, H. Riesemeier, Applied Physics Letters 90 (2007) 174105.

[17] C. Hartnig, I. Manke, R. Kuhn, N. Kardjilov, J. Banhart, W. Lehnert, Appl Phys Lett 92 (2008) 134106.

[18] I. Manke, C. Hartnig, N. Kardjilov, H. Riesemeier, J. Goebbels, R. Kuhn, P. Krüger, J. Banhart, Fuel Cells 10 (2010) 26-34.

[19] C. Hartnig, I. Manke, J. Schloesser, P. Krüger, R. Kuhn, H. Riesemeier, K. Wippermann, J. Banhart, Electrochem Commun 11 (2009) 1559-1562.

[20] W. Görner, M.P. Hentschel, B.R. Müller, H. Riesemeier, M. Krumrey, G. Ulm, W. Diete, U. Klein, R. Frahm, Nuclear Instruments and Methods in Physics Research Section A: Accelerators, Spectrometers, Detectors and Associated Equipment 467-468 (2001) 703-706.

[21] J. Banhart, Advanced Tomographic Methods in Materials Research and Engineering, Oxford University Press, Oxford, UK, 2008.

[22] B.L. Henke, E.M. Gullikson, J.C. Davis, Atom. Data Nucl. Data Tables 54 (1993) 181-342.

[23] H. Markötter, I. Manke, P. Krüger, T. Arlt, J. Haussmann, M. Klages, H. Riesemeier, C. Hartnig, J. Scholta, J. Banhart, Electrochem Commun 13 (2011) 1001-1004.

[24] D. Gerteisen, T. Heilmann, C. Ziegler, J Power Sources 177 (2008) 348-354.

[25] H. Markötter, R. Alink, J. Haußmann, K. Dittmann, T. Arlt, F. Wieder, C. Tötzke, M. Klages, C. Reiter, H. Riesemeier, J. Scholta, D. Gerteisen, J. Banhart, I. Manke, International Journal of Hydrogen Energy 37 (2012) 7757-7761.
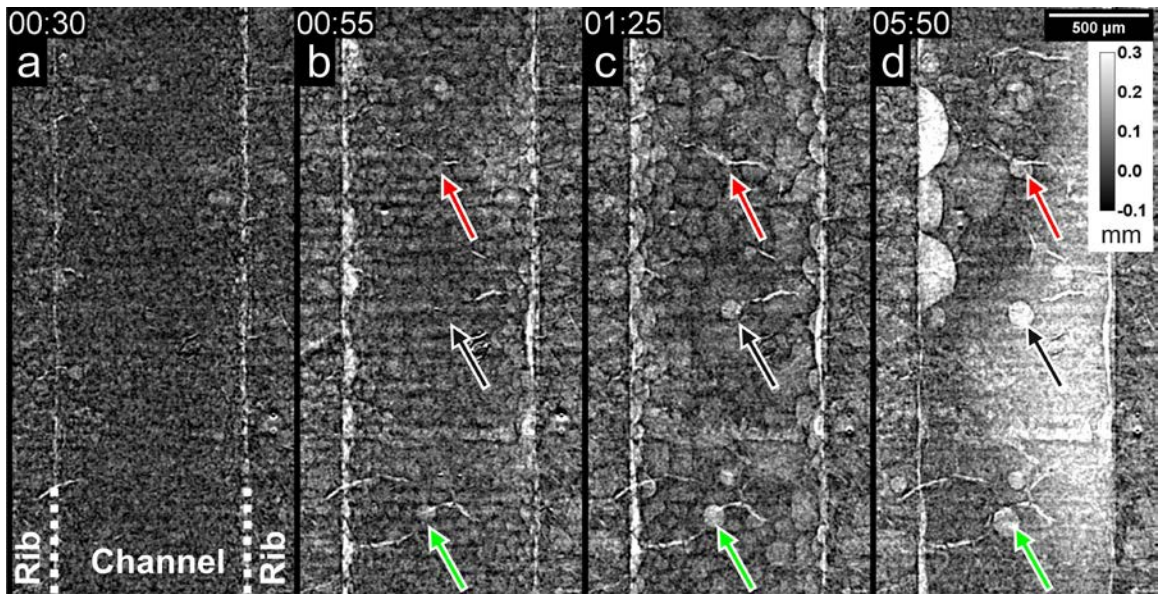
Fig. 1: Radiographic image series showing the water distribution in one channel. Water emerges at MPL cracks and eventually builds droplets in the channel.
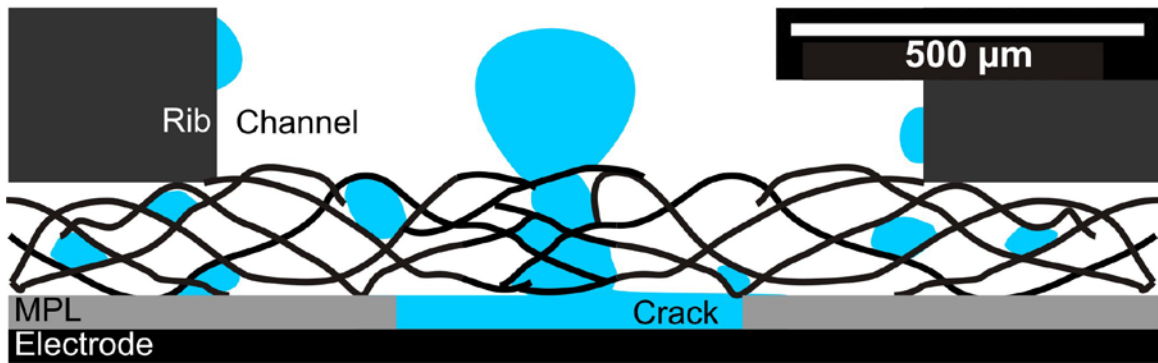
Fig. 2: Schematic cross section through the cell observed featuring a water filled crack in the MPL and a droplet in the channel situated at the GDL surface.
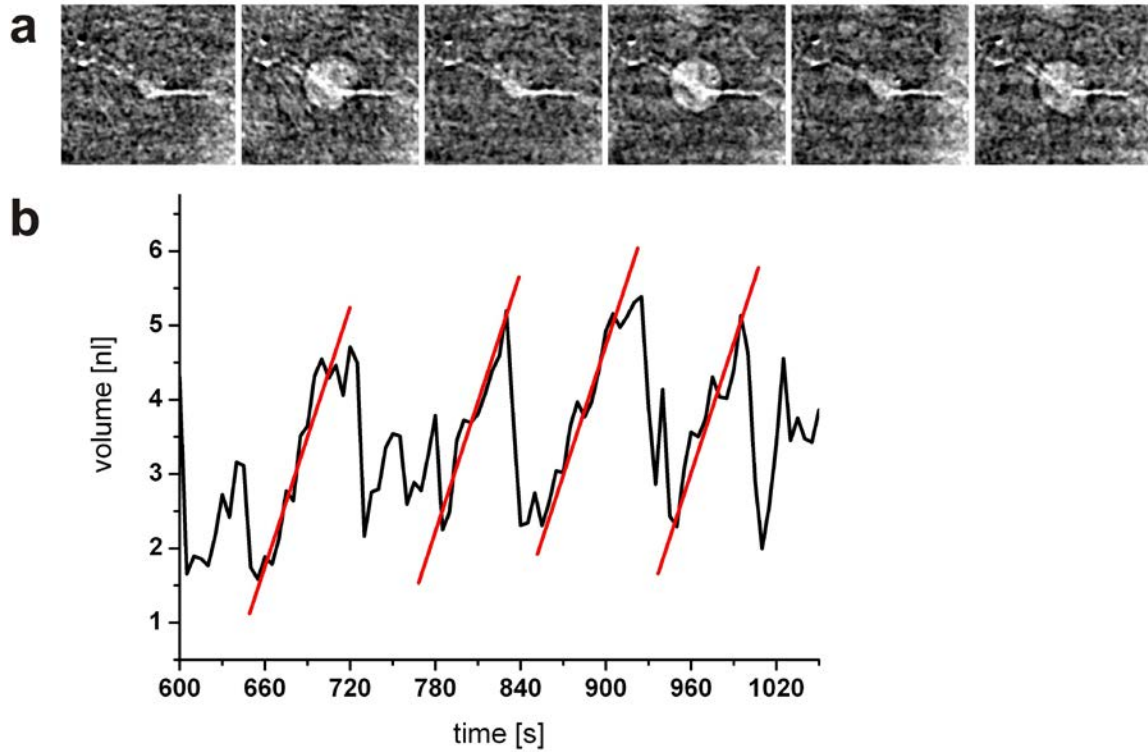
Fig. 3a: Periodic behavior of the droplet marked by red arrows in Fig. 1.
b: Dynamic volume quantification. The tendency of droplet growth is marked by red inclining lines.